

Immunological and mass spectrometry-based approaches to determine thresholds of the mutagenic DNA adduct *O*⁶-methylguanine *in vivo*

Alexander Kraus^{1,‡}, Maureen McKeague^{2,‡}, Nina Seiwert^{1,3}, Georg Nagel¹, Susanne M. Geisen², Nathalie Ziegler², Ioannis A. Trantakis², Bernd Kaina¹, Adam D. Thomas⁴, Shana J. Sturla², Jörg Fahrner^{1,3,*}

¹ Department of Toxicology, University Medical Center, Mainz, Germany

² Department of Health Sciences and Technology, ETH Zurich, Switzerland

³ Rudolf-Buchheim-Institute of Pharmacology, Justus-Liebig-University, Giessen, Germany

⁴ Centre for Research in Biosciences, University of the West of England, Bristol, UK

* Correspondence should be addressed to: Jörg Fahrner, PhD, Rudolf Buchheim Institute of Pharmacology, Justus-Liebig-University Giessen, Schubertstr. 81, D-35392 Giessen, Germany. Tel.: +49 (0)641 99-47603; Fax: +49 (0)641 99-47619; E-Mail: Joerg.Fahrner@pharma.med.uni-giessen.de

‡ authors contributed equally

RUNNING TITLE: Analysis of *O*⁶-methylguanine and threshold determination

KEY WORDS: *O*⁶-methylguanine, *O*⁶-methylguanine-DNA methyltransferase (MGMT), alkylating agents, ultra-performance liquid chromatography-tandem mass spectrometry, thresholds

CONFLICT OF INTEREST: The authors declare no conflict of interest.

ABSTRACT

N-nitroso compounds are alkylating agents, which occur widespread in diet and environment. They induce DNA alkylation adducts such as *O*⁶-methylguanine (*O*⁶-MeG), which is repaired by *O*⁶-methylguanine-DNA methyltransferase (MGMT). Persistent *O*⁶-MeG lesions have detrimental biological consequences like mutagenicity and cytotoxicity. Due to its pivotal role in the etiology of cancer and in cytotoxic cancer therapy, it is important to detect and quantify *O*⁶-MeG in biological specimens in a sensitive and accurate manner. Here, we used immunological approaches and established an ultra-performance liquid chromatography-tandem mass spectrometry (UPLC-MS/MS) to monitor *O*⁶-MeG adducts. First, colorectal cancer (CRC) cells were treated with the methylating anticancer drug temozolomide (TMZ). Immunofluorescence microscopy and an immuno-slot blot assay, both based on an adduct-specific antibody, allowed for the semi-quantitative, dose-dependent assessment of *O*⁶-MeG in CRC cells. Using the highly sensitive and specific UPLC-MS/MS, TMZ-induced *O*⁶-MeG adducts were quantified in CRC cells and even in peripheral blood mononuclear cells exposed to clinically relevant TMZ doses. Furthermore, all methodologies were used to detect *O*⁶-MeG in wildtype (WT) and MGMT-deficient mice challenged with the carcinogen azoxymethane. UPLC-MS/MS measurements and dose-response modeling revealed a non-linear formation of hepatic and colonic *O*⁶-MeG adducts in WT, whereas linear *O*⁶-MeG formation without a threshold was observed in MGMT-deficient mice. Collectively, the UPLC-MS/MS analysis is highly sensitive and specific for *O*⁶-MeG, thereby allowing for the first time for the determination of thresholds upon exposure to *O*⁶-methylating agents. We envision that this method will be instrumental to monitor the efficacy of methylating chemotherapy and to assess dietary exposures.

INTRODUCTION

Genotoxic *N*-nitroso compounds (NOC) are widespread in our diet and environment. They are found in processed meat and fish, beer, cosmetics and cigarette smoke (Fahrer and Kaina 2013). Furthermore, NOC are formed endogenously in the stomach and the large intestine by nitrosation of amino acids (Fahrer and Kaina 2013). These critical compounds cause DNA alkylation and thereby generate a plethora of DNA adducts, such as *N*-methylpurines and *O*⁶-methylguanine (*O*⁶-MeG) (Fu et al. 2012). *O*⁶-MeG is repaired by the suicide enzyme *O*⁶-methylguanine-DNA methyltransferase (MGMT) in a damage reversal reaction by transferring the methyl group from *O*⁶-MeG onto a cysteine residue located in its active site (Daniels et al. 2004). The S-methylation of MGMT leads to its inactivation and concomitant degradation by the ubiquitin-proteasome pathway (Xu-Welliver and Pegg 2002). Interestingly, a number of compounds modulate the MGMT level and its transferase activity. Antioxidants such as *N*-acetyl cysteine and the polyphenol curcumin were shown to increase MGMT activity (Niture et al. 2007), whereas the disulfide compound and dietary supplement α -lipoic acid (LA) was identified as natural MGMT inhibitor (Dörsam and Fahrer 2016; Göder et al. 2015). Importantly, persistent *O*⁶-MeG lesions have detrimental biological consequences including mutagenicity and carcinogenicity (Kaina et al. 2007). Apart from that, *O*⁶-MeG has also cytotoxic potential due to the downstream generation of DNA double-strand breaks (DSBs) (Mojas et al. 2007; Ochs and Kaina 2000; Quiros et al. 2010).

NOC-related compounds such as dimethylhydrazine and its metabolite azoxymethane (AOM) are frequently used in rodents to initiate colon carcinogenesis through induction of *O*⁶-MeG and other alkylated DNA bases (Neufert et al. 2007). Alkylating agents play also an important role in cancer chemotherapy due to their induction of cytotoxic DSBs, resulting mainly from subsequent replications over *O*⁶-MeG. These methylating anticancer drugs include temozolomide (TMZ) and dacarbazine (DTIC), which are both triazine compounds used for the treatment of high-grade glioma and malignant melanoma (Kaina et al. 2010).

Thus, understanding the basis of *O*⁶-MeG formation and how its repair is regulated are critical in broad biological questions, ranging from fundamental mechanisms of mutagenesis

to creating strategies to overcome clinical resistance to cancer therapeutics. However, gaining a functional and quantitative picture of how much O^6 -MeG is in genomic DNA from cells and tissues remains difficult. Immunological assays for detection of O^6 -MeG have been developed that are based upon a monoclonal antibody against the adduct (Seiler et al. 1993). This O^6 -MeG antibody has been used to visualize the DNA lesion in fixed cultured cells and organs, e.g. liver and colon, by immunofluorescence microscopy (Fahrer et al. 2015; Seiler et al. 1993). In addition, the antibody has been successfully employed for immuno-slot blot (ISB) analysis of O^6 -MeG lesions in genomic DNA extracted from cells and tissue (Fahrer et al. 2015; Mikhed et al. 2016; Stephanou et al. 1996), and an ELISA-related assay, in which single-stranded (ss) DNA fragments with O^6 -MeG were captured by the antibody followed by the detection of the ssDNA (Georgiadis et al. 2011). Complementary to immunoassay strategies, DNA adducts have been measured in diverse sample matrices by liquid chromatography combined with tandem mass spectrometry (LC-MS/MS). This approach was successfully used to quantify O^6 -MeG in lung and liver DNA ($\geq 50 \mu\text{g}$) from rats chronically exposed to 10 ppm of the tobacco-specific nitrosamine 4-(methylnitrosamino)-1-(3-pyridyl)-1-butanone (NNK), which worked with fresh-frozen and formalin-fixed paraffin-embedded tissue (Guo et al. 2016; Upadhyaya et al. 2009). By means of LC-MS/MS, the formation of O^6 -MeG was also monitored in calf thymus DNA and genomic DNA (100 μg) from colorectal cancer cells challenged *in vitro* with potassium diazoacetate at mM doses (Vanden Bussche et al. 2012).

Here, we performed a head-to-head comparison of these methods and examined the scope of each method for measuring O^6 -MeG adducts in both cells and tissues isolated from animals exposed to the anticancer drug TMZ and the colonotropic carcinogen AOM. Our data illustrated that both immunofluorescence (IF) and immunoslot blot (ISB) assay permitted the time- and dose-dependent detection of O^6 -MeG in CRC cells in a semi-quantitative manner, but are limited in sensitivity as illustrated in colon tissue exposed to low AOM doses. The UPLC-MS/MS approach was demonstrated to be highly sensitive and specific, allowing for the quantification of O^6 -MeG adducts in CRC cells and peripheral blood mononuclear

cells (PBMCs) at clinically relevant TMZ doses. Furthermore, the dose-response curve of AOM-induced O^6 -MeG formation was assessed by mass spectrometry in liver and colon tissue of mice differing in their MGMT repair status. Using hockey-stick dose-response modeling, our data revealed, for the first time, a genotoxic threshold for O^6 -MeG formation *in vivo*, resulting from MGMT repair activity.

MATERIAL AND METHODS

Material

All solutions were made with deionized water (18.2 MΩ resistivity). *O*⁶-methyl-d₃-guanine (*O*⁶-Me-d₃-G) was from Toronto Research Chemicals (Toronto, Canada). *O*⁶-MeG, ammonium hydroxide (ACS Reagent 28-30 %), hydrochloric acid (ACS Reagent 37 %), and acetic acid (HPLC grade) were purchased from Sigma-Aldrich (Buchs, Switzerland). Guanine was obtained from Acros Organics (New Jersey, USA) and Strata-X polymeric columns (30 μm) were from Phenomenex (Torrance, USA). Methanol (HPLC Gradient Grade) was bought at VWR (Dietikon, Switzerland).

Cell Culture

HCT116 colorectal cancer cells were kindly provided by Dr. Bert Vogelstein (John Hopkins University, Baltimore, USA). HCT116 cells were cultured in DMEM (Life Technologies, Darmstadt, Germany) supplemented with 10 % FCS and antibiotics (100 U/mL penicillin and 100 μg/mL streptomycin). PBMCs (peripheral blood mononuclear cells) were isolated from buffy coat by density centrifugation as described previously (Heylmann and Kaina 2016). Buffy coat from human healthy donors was provided by the blood transfusion center at University Medical Center, Mainz, Germany. Blood samples were layered on Histopaque (Sigma-Aldrich, Deisenhofen, Germany) and centrifuged at 2500 rpm for 35 min at RT without the brake. PBMCs (lymphocytes, monocytes) were collected, transferred to a 50 ml tube and resuspended in wash buffer (2 mM EDTA in PBS with 0.5% bovine serum albumin). Cells were pelleted by centrifugation and washed three times in wash buffer. Finally, cells were resuspended in X-VIVO 15 medium (LONZA, Basel, Switzerland) and transferred into six well plates.

Animal experiments

Mgmt-null (*MGMT*^{-/-}) mice on a C57BL/6 background were described previously (Bugni et al. 2009; Glassner et al. 1999). Eight to 14 week old *MGMT*^{-/-} and C57BL/6 wildtype (WT) mice

were used. All mouse strains were obtained from the in-house animal breeding facility at University Medical Center, Mainz, Germany. Animal experiments were approved by the government of Rhineland-Palatinate and the Animal Care and Use Committee of the University Medical Center, Mainz, Germany. All animal studies were performed in agreement with the German federal law and the guidelines for the protection of animals. Azoxymethane (AOM; Sigma, Deisenhofen, Germany) solution was prepared as described previously and administered by intraperitoneal injection at doses up to 10 mg/kg body weight (bw) (Fahrer et al. 2015). Animals were then sacrificed after 24 h. Colon and liver tissue were harvested, carefully rinsed with ice-cold PBS and either snap-frozen in liquid nitrogen or fixed in 4 % neutral buffered formaldehyde solution (Roti[®]-Histofix; Carl Roth, Karlsruhe, Germany). For subsequent histological analysis, fixed tissue was embedded in paraffin and stored at room temperature awaiting immunological analysis as detailed below.

Immunofluorescence detection of O⁶-MeG adducts

HCT116 cells (2×10^5 cells per well) were seeded onto cover slips and allowed to adhere overnight. The medium was replaced by fresh medium and the cells were then preincubated with the specific MGMT inhibitor O⁶-benzylguanine (O⁶-BG; 10 μ M; Sigma-Aldrich, Deisenhofen, Germany) for 2 h. Temozolomide (TMZ; kind gift of Dr. Geoffrey P. Margison, Manchester, UK) was added (0 to 1000 μ M) and cells were incubated for another 2 h. Following aspiration of the medium, cells were washed with pre-warmed phosphate-buffered saline (PBS) and fixed with ice-cold methanol for 15 min at -20 °C. After two washing steps with PBS, RNA was digested with a mixture of RNase A (200 μ g/ml) and RNase T (50 U/ml) for 10 min at 37 °C. Cells were washed with PBS followed by Proteinase K (20 μ g/ml) digestion for 10 min at 37 °C. Cells then were washed with 0.2 % glycine in PBS for 10 min and cover slips were transferred into a humid chamber. Unspecific binding sites were blocked with 5 % BSA in PBS for 45 min at RT. Subsequently, the samples were incubated with a primary mouse antibody against O⁶-MeG (diluted 1:2000 in 1 % BSA in tris buffered saline-tween 20 (TBS-T); #SQX-SQM003.1, Axxora, Farmingdale, USA) overnight at 4 °C.

After several washing steps with TBS-T and PBS, the samples were incubated with an appropriate secondary antibody (Goat-anti-Mouse-Alexa Fluor 488, diluted 1:400 in 1 % BSA/PBS, Life Technologies) for 2 h at RT under light exclusion. After several washing steps with TBS-T and PBS, the nuclei were counterstained with TO-PRO-3 (diluted 1:100 in PBS, Life Technologies, Darmstadt, Germany) for 15 min at RT. Finally, the cover slips were coated with Vectashield® (Linaris, Dossenheim, Germany) medium and transferred onto a microscope slide. The samples were analyzed by confocal microscopy with a Zeiss Axio Observer.Z1 microscope equipped with a LSM710 laser-scanning unit (Zeiss). Images were acquired with ZEN software and processed with ImageJ (NIH, USA). The mean O^6 -MeG intensity per nucleus was assessed with ImageJ (at least 10 sections with 100 nuclei/treatment, $n \geq 3$) and data were evaluated using GraphPad Prism 7.0 software.

Isolation of genomic DNA from cells and tissue

HCT116 cells (4×10^6) were seeded into 10 cm dishes and grown overnight. Cells were then incubated in fresh medium and O^6 -BG was added as described above. After 2 h, cells were treated with increasing doses of TMZ as indicated and harvested. To extract the genomic DNA, cells were resuspended in 300 μ l Tris-EDTA buffer supplemented with 0.1 % Triton X-100 and RNase A (30 μ g/ml). After incubation for 1.5 h at RT, proteinase K (20 μ g/ml) and 1 % SDS were added and incubated overnight at 48°C. In the next step, 700 μ l phenol/chloroform/isoamyl alcohol (Carl Roth, Karlsruhe, Germany) was added. The samples were briefly vortexed and centrifuged for 5 min at 20.000 g. The upper aqueous layer was transferred into a new reaction tube and extracted again with 700 μ l phenol-chloroform. Following centrifugation, the upper aqueous layer was transferred to a new reaction tube and supplemented with 750 μ l 90 % ethanol and 1 M NH_4OAc in order to precipitate the DNA for 1 h at 4 °C. The samples were then centrifuged for 45 min at 20. 000 g and 4 °C. The supernatant was discarded and the DNA pellets were washed with 1 ml 70 % EtOH. Following centrifugation at 20.000 g and 4 °C for 15 min, the supernatant was discarded and the remaining DNA pellets were dissolved in 50 – 100 μ l TE buffer. The samples were gently

vortexed and put on ice. Finally, the DNA content and purity were determined with a NanoDrop 2000 (Thermo Scientific, Dreieich, Germany).

PBMCs (6×10^6 ; approximately 70 % T-lymphocytes) in 2.5 ml X-Vivo 15 medium were exposed to increasing doses of TMZ (50 to 1000 μM) for 2 h at 37 °C. PBMCs were then transferred into tubes, washed with PBS and centrifuged for 5 min at 300 g. The supernatant was discarded and the pellets were resuspended in PBS. The cell suspension was centrifuged at 600 g for 5 min and pellets were processed to isolate genomic DNA as described above.

In order to isolate genomic DNA from mouse tissue, snap frozen colon and liver (~ 20 mg) were homogenized with a pestle and samples were processed as described above.

Immuno-slot blot assay (ISB) of O^6 -MeG adducts

A previously established immuno-slot blot assay (Göder et al. 2015) was used to determine O^6 -MeG adduct levels in genomic DNA extracted from TMZ-treated HCT116 cells or AOM-treated animals. First, 500 ng DNA in TE buffer was denatured by heating for 10 min at 99 °C. 50 μl of 2 M ammonium acetate were then added and samples were vortexed followed by their immediate vacuum-aspiration onto a positively charged nylon membrane (GE Healthcare, Munich, Germany). The membrane was fixed for 90 min at 90 °C and incubated for 60 min with blocking buffer (5 % dry milk in TBS-T). Subsequently, the membrane was incubated with a primary mouse antibody against O^6 -MeG (diluted 1:500 in 1 % BSA in TBS-T) overnight at 4 °C. After several washing steps with TBS-T, the membrane was incubated with a secondary peroxidase-coupled antibody (G- α -M-HRP, diluted 1:2000 in blocking buffer; Santa Cruz Biotechnology, Heidelberg, Germany) for 1 h at RT. After several washing steps with TBS-T, O^6 -MeG adducts were visualized by enhanced chemoluminescence detection using Western Lightning® Plus-ECL (Perkin Elmer, Rodgau, Germany). Densitometric evaluation of blots was conducted by Adobe Photoshop CS5 and analyzed by GraphPad Prism 7.0 software.

Immunohistochemistry (IHC)

Formalin-fixed, paraffin-embedded (FFPE) colon and liver tissue from AOM-treated mice were sectioned at 5 µm and processed for immunohistochemistry as reported (Fahrer et al. 2015). Tissue sections were incubated at 60 °C for 30 min in a drying oven, then deparaffinized in xylene and rinsed in graded ethanol solutions. Following several washing steps, the sections were immersed in pre-heated antigen retrieval solution (DAKO, Hamburg, Germany) for 30 min in a steamer. The samples were allowed to cool for 15 min at RT and washed several times in PBS. This process was followed by a permeabilization step in 0.4 % Triton X-100 in PBS for 5 min at RT. Sections were then rinsed in PBS and RNA digestion was performed for 1 h at 37 °C using both RNase A (200 µg/ml) and RNase T (50 U/ml).

After alkaline unwinding of the DNA for 5 min, the sections were carefully washed in PBS and incubated with Pepsin (60 µg/ml) 30 min at 37 °C. Thereafter, the sections were washed with PBS and incubated with proteinase K (20 µg/ml) for 30 min at 37 °C. Following another washing step with 0.2 % glycine-PBS, the sections were incubated for 2 h with blocking solution (DAKO, Hamburg, Germany) at RT. The sections were then treated with an *O*⁶-MeG antibody (1:100, diluted in 2 % BSA in PBS) overnight at 4 °C. After several washing steps in PBS-0,1 % Tween, the samples were incubated with the appropriate secondary antibody (G-α-M-Alexa 488, 1:500 diluted in 2 % BSA in PBS/0.2 % Triton X-100; Life Technologies, Darmstadt, Germany) for 2 h at RT. The sections were then rinsed thoroughly with PBS-T 0.1 % and a nuclear staining was performed using TO-PRO-3 (1:100 in PBS) for 30 min at RT. Slides were mounted with Vectashield[®] medium and analyzed by confocal microscopy with a Zeiss Axio Observer.Z1 microscope equipped with a LSM710 laser-scanning unit (Zeiss, Oberkochen, Germany). Images were processed with ImageJ version 1.45 (NIH, USA).

LC-MS/MS analysis of *O*⁶-MeG adducts

DNA hydrolysis

All DNA samples were measured on a Nanodrop 1000 (PeqLab, Rodgau, Germany). The total number of nucleotides present was calculated based on the average base pair molecular weight of 650 g/mol. The number of guanine residues was calculated assuming 21 % guanine in the mouse genome, and 20.5 % in the human genome (Ruvinsky and Graves 2005). A minimum of 10 µg of DNA was transferred to new Eppendorf DNA LoBind microcentrifuge tubes and concentrated to dryness by vacuum centrifugation. Samples were resuspended and thoroughly vortexed in 500 µL of a 0.1 M HCl solution spiked with 2 nM of the internal standard (IS), O^6 -Me- d_3 -G. To release the purines from the DNA, each sample was heated for 2 h at 70 °C. Samples were cooled at RT for at least 10 min followed by a 20 s centrifugation pulse at 1000 g. Each sample was neutralized with 15 µL of 15 % aqueous ammonium hydroxide (NH₄OH) and vortexed.

Confirmation of DNA hydrolysis

30 µL from each DNA sample was removed for HPLC analysis to verify complete release of guanine. Quantification of guanine was carried out on an Agilent Technologies 1200 Series HPLC (Santa Clara, CA) with a UV-visible detector. The method was adapted from Roy *et al.* (Roy *et al.* 2013). To monitor absorbance, the diode array detector was set to 270 nm and the reference was set to 360 nm.

Chromatography was performed with a Luna C18 Column (5 µm, 100 Å, 4.6 x 250 mm) from Phenomenex (Torrance, CA). Mobile phase A was water and mobile phase B was methanol. The flow rate was 1 mL/min and the column temperature was not controlled. 8 µL of sample was injected and separated as follows: 1 % B for 3 min, 1–10 % B linear gradient for 7 min, a wash at 85 % B for 3 min, and re-equilibration at 1 % B for 7 min (20 min total run time). Guanine eluted at a RT of 8.7 min. Samples were analyzed in duplicate.

A calibration curve for guanine (2-100 µM) was prepared in a 0.1 M HCl, 0.03 % NH₄OH solution. The amount of guanine in each sample was calculated on the basis of guanine peak area, slope of the calibration curve, and fraction of the total volume injected. The percent recovery of guanine was calculated using the guanine measured by HPLC compared to the

theoretical amount calculated from the Nanodrop measurement. All samples yielded between 80-120% recovery of released guanine.

Adduct enrichment

Solid phase extraction (SPE) columns (Strata-X 33 μm , 30 mg/1 mL) were preconditioned with two 1 mL washes with methanol, followed by three separate washes of 1 mL water each. The entire remaining sample (485 μL) was loaded onto a column for enrichment and purification. Each column was then washed with 600 μL water, then 600 μL of 3 % methanol. Elution was performed by adding 600 μL of 60 % methanol. The entire eluent was recovered and vacuum centrifuged to dryness in 250 μL conical glass HPLC inserts. Samples were stored at -20 °C. Immediately prior to LC-MS/MS analysis, samples were thawed, reconstituted in 20 μL water, and sonicated for 10 min.

LC-ESI-MS/MS

Samples were analyzed by LC-MS/MS using a nanoAcquity UPLC system (Waters, Milford, CA) and Agilent tandem quadrupole mass spectrometer (LCQ Vantage, Thermo Scientific, Waltham, MA) with an electrospray ionization source (ESI). Mass spectrometry ionization parameters were optimized by tuning the instrument with 1 μM O^6 -MeG, O^6 -d3-MeG, and G by direct injection. The ESI source was set in positive ion mode with the following parameters: capillary temperature, 270 °C; spray voltage, 3000 V; sheath gas pressure, 25; ion sweep gas pressure, 0; aux gas pressure, 5; Q2 CID gas pressure, 1.5 mTorr; collision gas, argon; scan width, m/z 0.01; scan time, 0.1 s. Optimal collision energies for each transition are in Table 1.

Chromatography was performed with a Synergi 4 μm Polar-RP column (Phenomenex 80 Å 150 x 0.5 mm). Mobile phases were sonicated for 15 min prior to the run. Mobile phase A was water with 0.05 % acetic acid, phase B was methanol, and the flow rate was 10 $\mu\text{L}/\text{min}$ at the column temperature was set to 40 °C. The autosampler was cooled to 4 °C, a seal wash was performed every 30 min, and the injection volume was 1 μL . Samples were

separated as follows: 0 % B for 1 min, 1–40 % B gradient for 14 min, 99 % B for 5 min, and re-equilibrate for 15 min. The eluent was directed to the MS between 2 min and 14 min, otherwise the eluent was diverted to the waste. O^6 -MeG and O^6 -d3-MeG eluted at 9.8 min. The single reaction monitoring (SRM) transitions that were monitored are listed in Table 1. Xcalibur software (Thermo) was used for data acquisition and processing.

Calibration curves

A series of 8 different O^6 -MeG standards of known concentration (0.5, 1, 2.5, 5, 10, 25, 40, 50 nM) was prepared. A fresh 20 μ L aliquot of each prepared standard was concentrated to dryness by vacuum centrifugation and resuspended in 500 μ L of a 0.1 M HCl solution spiked with 2 nM of the IS as above. Thermal acid hydrolysis and SPE were performed in the same way as the DNA samples. Standards were reconstituted with 20 μ L water for LC-MS/MS analysis. Each calibrated standard was measured in triplicate. Standards were prepared and analyzed immediately prior to analysis. The peak area ratio was determined for each standard by dividing the peak area of the standard by the peak area of the IS. Data were fitted to a straight line by least-squares (ordinary) in GraphPad Prism 7.0.

Adduct quantification

Each sample was first injected once into the MS to ensure they were within the linear range. For samples that were higher than the standard curve, a 1:10 dilution was performed in water. For samples where the O^6 -MeG was lower than the standard curve, the injection volume was increased to 4 μ L or was analyzed using a nanoAcquity UPLC M-class system (Waters, Milford, CA) and tandem quadrupole mass spectrometer (TSQ Quantiva, Thermo Scientific, Waltham, MA) with an electrospray ionization source (ESI) at the Functional Genomics Center Zürich using the same ionization parameters and chromatography. After adjusting these samples, at least one more technical replicate was performed. Acceptable precision for each sample was required, where the relative standard deviations of the technical triplicates was less than 20 %. The peak area ratio was determined for each

sample by dividing the peak area of the O^6 -MeG by the peak area of the O^6 -d3-MeG. The amount of O^6 -MeG in each sample was calculated using the peak area ratio, the slope of the calibration curve, and the fraction of the total volume injected. Sample quantification was then converted and reported as adducts per 10^7 total nucleotides.

Statistics

Experiments were performed independently three times, unless otherwise stated. Figures show representative images. Values are depicted as mean \pm standard errors of the mean (SEM) using GraphPad Prism 7.0 Software. Statistical analysis was performed using two-sided Student's t-test and statistical significance was defined as $p < 0.05$.

Hockey stick dose-response modelling

Dose-response modelling was performed as described (Lutz and Lutz 2009) using R software (version 3.3.1) (R Development Core Team 2013). The lower confidence interval of the threshold dose is also reported. It should be noted that confidence intervals of <0 lacks statistical significance for a threshold.

RESULTS

In this study, levels of O^6 -MeG resulting from exposure to either the anticancer drug TMZ or the colonotropic carcinogen AOM were evaluated in CRC cells and different murine tissue (*i.e.* liver and colon) by a combination of qualitative immunological assays and quantitative mass spectrometry (Fig. 1A). AOM requires metabolic activation by the hepatic enzyme CYP2E1 to generate a reactive methylating agent (Neufert et al. 2007). TMZ, on the other hand, spontaneously decomposes at neutral pH to deliver a methyl group (Zhang et al. 2012). Both chemicals give rise to DNA reactive methyldiazonium ions that induce the minor lesion O^6 -MeG among other DNA methylation adducts. The workflow of sample processing and subsequent analysis is depicted in Fig. 1B.

Time-dependent formation of O^6 -MeG in cells challenged with TMZ

First, we investigated the induction and persistence of O^6 -MeG in a time-dependent manner over 24 h. To this end, HCT116 CRC cells were pre-incubated with O^6 -BG for 2 h in order to inactivate MGMT and then challenged with TMZ for up to 24 h. Confocal IF microscopy showed a time-dependent formation of O^6 -MeG with a peak after 4 h, which persisted up to 14 h after exposure to TMZ (Fig. 2A and B). After 24 h, the O^6 -MeG level declined, presumably because of resynthesis of MGMT or lesion dilution resulting from cell division. To quantify the adducts, we used stable isotope dilution mass spectrometry. The results showed a similar time course of O^6 -MeG accumulation as compared to the IF analysis (Fig. 2C). 4 h after treatment with 500 μ M TMZ, the basal O^6 -MeG level (~ 2 lesions per 10^7 nucleotides) increased to 116 O^6 -MeG adducts per 10^7 nucleotides. After 24 h, the O^6 -MeG content decreased to 58 adducts per 10^7 nucleotides, which is still considerably higher than in untreated control cells. Representative chromatograms for O^6 -MeG measurements in TMZ-treated HCT116 cells are also shown (SI, Fig. 1). In order to illustrate the intrinsic MGMT repair capacity in HCT116 cells, cells were incubated in the absence or presence of the MGMT inhibitor O^6 -BG and challenged with 500 μ M TMZ (Fig. 2D). Mass spectrometry revealed a slightly higher, yet not statistically significant O^6 -MeG level following TMZ

treatment in cells pre-treated with the MGMT inhibitor (74 vs. 56 adducts per 10^7 nucleotides), indicating the protection mediated by MGMT against TMZ-induced O^6 -MeG in HCT116 cells.

Dose-dependent induction of O^6 -MeG in cells challenged with TMZ

In order to monitor the dose-dependent formation of O^6 -MeG adducts, HCT116 cells were pre-incubated with the pharmacological inhibitor O^6 -BG to block MGMT activity. The cells were then exposed to increasing doses of TMZ (0 – 1000 μ M) for 2 h, fixed and processed. O^6 -MeG was specifically labeled with an antibody followed by confocal microscopy (Fig. 3). As expected, O^6 -MeG displayed exclusive nuclear localization. TMZ, at 100 μ M, caused a moderate, significant rise in the O^6 -MeG level relative to the untreated control (Fig. 3A -C). At higher dose levels, O^6 -MeG levels increased dose-dependently (Fig. 3A - C). Subsequently, we compared the sensitivity of the ISB assay with mass spectrometry-based analysis of O^6 -MeG adducts in genomic DNA from TMZ-treated HCT116 cells. By means of the ISB assay, we were able to detect a dose-dependent O^6 -MeG DNA adduct formation, reaching statistical significance only at doses \geq 500 μ M TMZ (Fig. 4A and B). Doses up to 250 μ M were hardly distinguishable from the background level (Fig. 4B). In contrast, UPLC-MS/MS revealed a significant rise in O^6 -MeG at a lower dose of 100 μ M TMZ with 13 adducts per 10^7 nucleotides, while the baseline level without TMZ treatment was low (\sim 2.5 adducts per 10^7 nucleotides) (Fig. 4C). This clearly demonstrates the higher sensitivity and specificity of the mass spectrometry-based approach. It is interesting to note that we were also able to measure O^6 -MeG in PBMC following *in vitro* treatment with 100 μ M TMZ (SI Tab. 1). This experiment was conducted without the MGMT inhibitor O^6 -BG, *i.e.* in the presence of intrinsic MGMT repair activity.

Assessment of O^6 -MeG in tissue of AOM-treated mice and impact of MGMT

Having extensively characterized the dose- and time-dependent formation of O^6 -MeG in CRC cells, we switched to a mouse model using B6/J wild type (WT) and transgenic, MGMT

deficient mice (MGMT^{-/-}). The animals were exposed to AOM, which is a well-established colonotropic carcinogen. AOM requires metabolic activation in the liver and the colorectum, involving an interplay of hepatic cytochrome P450 2E1 (CYP2E1)- and UDP-glucuronosyl-transferase (UGT)-dependent metabolism together with β -glucuronidase activity from gut bacteria (Neufert et al. 2007). AOM was administered by intraperitoneal injection in doses ranging from 0 – 10 mg/kg bw and animals were sacrificed after 24 h to isolate genomic DNA from liver and colorectal tissue. O⁶-MeG levels were already assessed in our previous work using the ISB technique (Fahrer et al. 2015). Both genotypes displayed a dose-dependent formation of hepatic O⁶-MeG adducts, with significant higher levels in MGMT k.o. mice that lack methyl transferase activity towards O⁶-MeG (Fahrer et al. 2015). In colorectal tissue, no differences in O⁶-MeG levels were detected in WT mice challenged with up to 10 mg/kg AOM, while a dose-dependent increase was observed in MGMT-deficient mice using the ISB assay (SI Fig. 2A and B). Next, the liver samples were analyzed by mass spectrometry, resulting in dose-dependent generation of O⁶-MeG as a function of the repair phenotype (Fig. 5A and C). It should be stressed that O⁶-MeG levels were about two-fold higher in MGMT^{-/-} as compared to WT animals at doses of 3 and 5 mg AOM/kg bw (SI Fig. 3A), reaching statistical significance only for 5 mg. Finally, we studied O⁶-MeG formation in colorectal tissue, which is pivotal for DNA alkylation-triggered colorectal carcinogenesis. Intriguingly, UPLC-MS/MS revealed O⁶-MeG induction (~ 6 adducts per 10⁷ nucleotides) at the lowest tested AOM dose (3 mg AOM/kg bw) in WT animals, which was tremendously augmented (~ 60 adducts per 10⁷ nucleotides) at the highest AOM dose (10 mg/kg bw) (Fig. 5E). In stark contrast, MGMT^{-/-} animals displayed a dose-dependent and almost linear formation of O⁶-MeG adducts (16, 35, 81 adducts per 10⁷ nucleotides, respectively) (Fig. 5G). Side-by-side comparison of the induced O⁶-MeG lesions in colorectal tissue showed significantly higher levels in MGMT^{-/-} versus WT animals at AOM doses \leq 5 mg/kg bw (SI Fig. 3B).

Dose-response modeling of O⁶-MeG adducts and threshold analysis

We performed hockey stick dose-response modeling (Lutz and Lutz 2009) on the *in vivo* data following ISB and MS quantification of O^6 -MeG adducts to identify a potential threshold dose and assess the dose-response relationship (Fig. 5 B, D, F and H). We only identified a threshold dose using UPLC-MS/MS quantification, but not via ISB (SI Fig. 4). Interestingly, the threshold dose of 1.9 mg/kg bw and 4.8 mg/kg bw AOM in the respective liver and colon of WT mice was absent in the MGMT-deficient genotype (Tab. 2), indicating a change in dose-response relationship from sub-linear to linear when MGMT-mediated repair of O^6 -MeG is lacking.

DISCUSSION

The present work provides a characterisation of the currently available techniques to detect and quantify O^6 -MeG adducts in cells and murine tissues, with a focus on their sensitivity and specificity. Furthermore, the approaches were applied to determine genotoxic thresholds using the hockey-stick dose-response modeling. First, we showed that IF microscopy allows for the time- and dose-dependent detection of O^6 -MeG in cells treated with the methylating antineoplastic drug TMZ. The procedure itself is relatively fast and not expensive, but includes critical steps such as the unwinding of DNA at alkaline pH, during which the cells can detach. Furthermore, the used O^6 -MeG antibody caused some background signal, which is particularly prominent in tissue samples (SI, Fig. 5). The digestion of proteins and RNA are further essential steps to yield specific, nuclear staining of O^6 -MeG. This method has been employed to detect O^6 -MeG in cells and in tissue, particularly liver and colon tissue (Fahrer et al. 2015; Nyskohus et al. 2013), as it offers the advantage to visualize damage induction in distinct cell types and regions within a given tissue. Using confocal microscopy, we could demonstrate the spatial formation of O^6 -MeG adducts in liver lobuli, with the highest damage induction in hepatocytes around the central hepatic vein, while no adducts were formed in the periportal field (SI Fig. 5 and (Fahrer et al. 2015)). Interestingly, O^6 -MeG staining can also be combined with the detection of γ H2AX, an established marker for DNA DSBs (Fahrer et al. 2014; Kinner et al. 2008), in paraffin-embedded liver tissue (Fahrer et al. 2015). The IF-based method proved also to be useful for monitoring the time-dependent induction and removal of O^6 -MeG adducts in colon crypts of rats treated with up to 15 mg AOM/kg bw (Nyskohus et al. 2013). However, IF is a semi-quantitative method and offers moderate sensitivity as compared to mass spectrometry, which was revealed mainly during the analysis of tissue samples. For example, our UPLC-MS/MS approach detected O^6 -MeG in liver tissue of WT mice at low AOM doses (Fig. 5), whereas IF microscopy did not (Fahrer et al. 2015).

Second, we employed the ISB assay to detect O^6 -MeG adducts in genomic DNA isolated from cells and tissues exposed to methylating agents. The ISB assay allows for the direct comparison of multiple samples (up to 48) on the same membrane, requiring only little amount of DNA (≤ 500 ng). Furthermore, it is a very fast and inexpensive method. We showed a dose-dependent O^6 -MeG generation in cells challenged with TMZ, however with only moderate sensitivity. Nevertheless, O^6 -MeG adducts were monitored in liver DNA from WT and MGMT-deficient mice exposed to low dose levels of AOM (3 mg/kg bw). It also should be mentioned that the effect of the different DNA repair phenotype, *i.e.* MGMT proficiency and MGMT deficiency, was clearly visible here. In support of its rather moderate sensitivity, no AOM-dependent formation of O^6 -MeG was detectable in DNA isolated from colorectal tissue of WT animals using the ISB assay (SI Fig. 2). The method has also been applied to measure O^6 -MeG and O^6 -ethylguanine in human lymphocytes exposed to methylnitrosurea (MNU) and ethylnitrosurea (ENU), respectively, at the mM dose range (0.5 – 4 mM) *in vitro* (Jiao et al. 2007; Stephanou et al. 1996), confirming the limited sensitivity of ISB. This drawback is also attributable to the background signal, which is observed in untreated control samples.

Third, we applied UPLC-MS/MS to quantify O^6 -MeG adduct levels in human cells and murine tissue samples (liver and colon). This approach was highly sensitive and superior to the other antibody-based methods (IF and ISB) throughout our experiments. While former studies using HPLC-MS/MS required moderate to high amounts of DNA (50 μ g up to 1 mg) (Upadhyaya et al. 2009; Vanden Bussche et al. 2012; Zhang et al. 2006), we have optimized the sample cleanup and subsequent analysis, reducing the amount of DNA needed to below 10 μ g. Our UPLC-MS/MS approach is highly sensitive and permitted the detection of O^6 -MeG in colorectal tissue of WT mice challenged with only 3 mg/kg bw AOM. This method was also instrumental for our very recent study dealing with the impact of the DNA repair protein PARP-1 on alkylation-induced colorectal carcinogenesis (Dörsam et al. 2018).

Furthermore, mass spectrometry revealed moderate differences in O^6 -MeG levels following TMZ treatment in the presence or absence of the MGMT inhibitor O^6 -BG, which were however not statistically significant. This finding could be attributable to several factors. First, HCT116 cells display only moderate MGMT activity (Göder et al. 2015), whereas other CRC cells such as HT29 have a 4-fold higher MGMT activity (Tomaszowski et al. 2015). Less O^6 -BG is thus required to inhibit the cellular MGMT pool in HCT116 cells, attenuating the effects particularly at a high TMZ dose of 500 μ M. Second, it is conceivable that TMZ at high doses directly alkylates the catalytic Cys residue of MGMT, which could also overshadow the O^6 -BG-mediated inhibition. Third, the TMZ exposure time used for this experiment (2 h) might be not ideal, bearing in mind that O^6 -MeG induction by TMZ peaks after 4 h (Fig. 2C).

Intriguingly, our measurements revealed a linear, dose-dependent accumulation of adducts in MGMT deficient mice, whereas adduct levels exhibited non-linearity in WT animals, and the threshold analysis supports this result (Tab. 2). We found threshold doses of AOM in the liver and colon of treated mice at 1.93 mg/kg bw and 4.78 mg/kg bw, respectively. The liver has higher basal levels of the AOM activating enzyme, CYP2E1, than in the colon (Rosenberg and Mankowski 1994). We could therefore hypothesize that more AOM is activated in the liver and able to react with DNA, accounting for the lower threshold dose than in the colon. Caution is urged however, as the dose-responses look sub-linear (due to vastly higher adduct levels at the highest dose) as oppose to threshold, particularly in the colon (Figure 5). However, the difference in threshold dose between the repair phenotypes is intriguing and supports a mechanistic basis for the observed threshold doses (Fahrer et al. 2015; Thomas et al. 2013).

Moreover, it is hypothesised that detoxifying processes can prevent genotoxin activation, subsequent DNA reaction and adduct formation and, therefore, contribute to a non-linear DNA adduct relationship (Thomas et al. 2015). The half-life of the DNA adducts (governed by their removal by repair enzymes, such as MGMT) may influence the relationship observed

depending on the time following treatment when the adducts were quantified. The influence of DNA repair is evidenced in the absence of threshold doses in the MGMT-deficient phenotype. While this data is limited and firm conclusions on the dose-responses are difficult to draw, it is interesting to speculate particularly, as in this instance, the relationships correlate to our mechanistic understanding of DNA damage induction and repair. This is consistent with our previous study dealing with the impact of DNA repair on the dose-response relationship in alkylation-induced colorectal carcinogenesis (Fahrer et al. 2015) and illustrates that initial DNA adduct levels may be correlated with later onset of tumorigenesis.

Using this mass-spectrometry-based approach, O^6 -MeG formation was also quantitatively assessed in PBMCs isolated from healthy human volunteers following *in vitro* treatment with the anticancer drug TMZ. This experiment was conducted without the MGMT inhibitor O^6 -BG, i.e. in the presence of intrinsic MGMT activity that amounts to about 105 fmol/10⁶ PBMCs (Janssen et al. 2001). Interestingly, significant levels of O^6 -MeG were detected at a dose of 100 μ M TMZ, which is comparable to the plasma concentration that can be achieved in patients after oral administration of the drug (Britten et al. 1999; Hammond et al. 1999). It can be envisioned that O^6 -MeG induced by methylating anticancer drugs such as TMZ and DTIC could be monitored in peripheral blood cells as clinical pharmacodynamic biomarker in the future, comparable to γ H2AX and poly(ADP-ribose) as proposed elsewhere (Redon et al. 2010). This will assist in stratifying patients and monitoring therapeutic efficacy in personalized medicine, an approach that is also amenable to other DNA damaging anticancer drugs, including cis-platin and cyclophosphamide (Storretta et al. 2017). The advantages and disadvantages of each method used here are summarized in Table 3.

Very recently, novel strategies have been developed to detect O^6 -MeG in a sequence-specific context. To this end, artificial nucleotides (benzimidazole-derived 2'-deoxynucleoside-5'-O-triphosphates) have been synthesized, which are incorporated into DNA opposite O^6 -MeG by an engineered KlenTaq DNA polymerase (Wyss et al. 2016). Novel hybridization

probes based on an oligonucleotide with nucleoside analogues conjugated to gold nanoparticles have also been used to successfully detect O^6 -MeG within a mutational hotspot in the *KRAS* oncogene (Trantakis et al. 2016). These chemical approaches may open a new avenue to measure O^6 -MeG levels in a sequence-specific manner at single base resolution instead of assessing the global O^6 -MeG load in genomic DNA.

In summary, the UPLC-MS/MS approach allowed for the quantitative, sensitive and specific detection of critical O^6 -MeG adducts in cells and tissue. This technique was further pivotal for the determination of threshold levels for O^6 -MeG adducts, which were caused by the repair enzyme MGMT. We envision that this method will be instrumental to monitor the therapeutic efficacy of alkylating anticancer drugs and to assess dietary and environmental exposure to O^6 -MeG-inducing agents.

ACKNOWLEDGEMENT

This work was supported by the University Medical Center Mainz (MAIFOR) and the German Research Foundation (DFG-FA1034/3-1 and DFG-KA724/29-1). We are indebted to Dr. Daniel Heylmann (Department of Toxicology, University Medical Center, Mainz, Germany) for isolating PBMCs from buffy coat. We are also grateful to Dr. Bert Vogelstein (John Hopkins University, Baltimore, USA) for providing HCT116 cells, to Dr. Leona D. Samson (MIT, Boston, USA) for providing MGMT knockout animals, and to Dr. Geoffrey P. Margison (University of Manchester, UK) for providing TMZ. We also thank the FGCZ Functional Genomics Center Zürich (FGCZ) for LC-MS/MS assistance.

REFERENCES

- Britten CD, Rowinsky EK, Baker SD, et al. (1999) A Phase I and pharmacokinetic study of temozolomide and cisplatin in patients with advanced solid malignancies. *Clin Cancer Res* 5(7):1629-37
- Bugni JM, Meira LB, Samson LD (2009) Alkylation-induced colon tumorigenesis in mice deficient in the Mgmt and Msh6 proteins. *Oncogene* 28(5):734-41 doi:10.1038/onc.2008.426
onc2008426 [pii]
- Daniels DS, Woo TT, Luu KX, et al. (2004) DNA binding and nucleotide flipping by the human DNA repair protein AGT. *Nat Struct Mol Biol* 11(8):714-20 doi:10.1038/nsmb791
- Dörsam B, Fahrner J (2016) The disulfide compound alpha-lipoic acid and its derivatives: A novel class of anticancer agents targeting mitochondria. *Cancer Lett* 371(1):12-9 doi:10.1016/j.canlet.2015.11.019
- Dörsam B, Seiwert N, Foersch S, et al. (2018) PARP-1 protects against colorectal tumor induction, but promotes inflammation-driven colorectal tumor progression. *Proc Natl Acad Sci U S A* 115(17):E4061-E4070 doi:10.1073/pnas.1712345115
- Fahrner J, Frisch J, Nagel G, et al. (2015) DNA repair by MGMT, but not AAG, causes a threshold in alkylation-induced colorectal carcinogenesis. *Carcinogenesis* 36(10):1235-44 doi:10.1093/carcin/bgv114
- Fahrner J, Huelsenbeck J, Jaurich H, et al. (2014) Cytotoxic distending toxin (CDT) is a radiomimetic agent and induces persistent levels of DNA double-strand breaks in human fibroblasts. *DNA Repair (Amst)* 18:31-43 doi:10.1016/j.dnarep.2014.03.002
- Fahrner J, Kaina B (2013) O6-methylguanine-DNA methyltransferase in the defense against N-nitroso compounds and colorectal cancer. *Carcinogenesis* 34(11):2435-42 doi:10.1093/carcin/bgt275
- Fu D, Calvo JA, Samson LD (2012) Balancing repair and tolerance of DNA damage caused by alkylating agents. *Nat Rev Cancer* 12(2):104-20 doi:10.1038/nrc3185
nrc3185 [pii]
- Georgiadis P, Kaila S, Makedonopoulou P, et al. (2011) Development and validation of a new, sensitive immunochemical assay for O(6)-methylguanine in DNA and its application in a population study. *Cancer Epidemiol Biomarkers Prev* 20(1):82-90 doi:10.1158/1055-9965.EPI-10-0788
- Glassner BJ, Weeda G, Allan JM, et al. (1999) DNA repair methyltransferase (Mgmt) knockout mice are sensitive to the lethal effects of chemotherapeutic alkylating agents. *Mutagenesis* 14(3):339-47
- Göder A, Nagel G, Kraus A, et al. (2015) Lipoic acid inhibits the DNA repair protein O6-methylguanine-DNA methyltransferase (MGMT) and triggers its depletion in colorectal cancer cells with concomitant autophagy induction. *Carcinogenesis* 36(8):817-31 doi:10.1093/carcin/bgv070
- Guo J, Yun BH, Upadhyaya P, et al. (2016) Multiclass Carcinogenic DNA Adduct Quantification in Formalin-Fixed Paraffin-Embedded Tissues by Ultraperformance Liquid Chromatography-Tandem Mass Spectrometry. *Anal Chem* 88(9):4780-7 doi:10.1021/acs.analchem.6b00124
- Hammond LA, Eckardt JR, Baker SD, et al. (1999) Phase I and pharmacokinetic study of temozolomide on a daily-for-5-days schedule in patients with advanced solid malignancies. *J Clin Oncol* 17(8):2604-13 doi:10.1200/JCO.1999.17.8.2604
- Heylmann D, Kaina B (2016) The gammaH2AX DNA damage assay from a drop of blood. *Sci Rep* 6:22682 doi:10.1038/srep22682
- Janssen K, Eichhorn-Grombacher U, Schlink K, Nitzsche S, Oesch F, Kaina B (2001) Long-time expression of DNA repair enzymes MGMT and APE in human peripheral blood mononuclear cells. *Arch Toxicol* 75(5):306-12
- Jiao L, Chang P, Firozi PF, Lai D, Abbruzzese JL, Li D (2007) Polymorphisms of phase II xenobiotic-metabolizing and DNA repair genes and in vitro N-ethyl-N-nitrosourea-induced O6-ethylguanine levels in human lymphocytes. *Mutat Res* 627(2):146-57 doi:10.1016/j.mrgentox.2006.11.001
- Kaina B, Christmann M, Naumann S, Roos WP (2007) MGMT: key node in the battle against genotoxicity, carcinogenicity and apoptosis induced by alkylating agents. *DNA Repair (Amst)* 6(8):1079-99 doi:S1568-7864(07)00124-3 [pii]
10.1016/j.dnarep.2007.03.008
- Kaina B, Margison GP, Christmann M (2010) Targeting O(6)-methylguanine-DNA methyltransferase with specific inhibitors as a strategy in cancer therapy. *Cell Mol Life Sci* 67(21):3663-81 doi:10.1007/s00018-010-0491-7

- Kinner A, Wu W, Staudt C, Iliakis G (2008) Gamma-H2AX in recognition and signaling of DNA double-strand breaks in the context of chromatin. *Nucleic Acids Res* 36(17):5678-94 doi:10.1093/nar/gkn550
- Lutz WK, Lutz RW (2009) Statistical model to estimate a threshold dose and its confidence limits for the analysis of sublinear dose-response relationships, exemplified for mutagenicity data. *Mutat Res* 678(2):118-22 doi:10.1016/j.mrgentox.2009.05.010
- Mikhed Y, Fahrner J, Oelze M, et al. (2016) Nitroglycerin induces DNA damage and vascular cell death in the setting of nitrate tolerance. *Basic Res Cardiol* 111(4):52 doi:10.1007/s00395-016-0571-4
- Mojas N, Lopes M, Jiricny J (2007) Mismatch repair-dependent processing of methylation damage gives rise to persistent single-stranded gaps in newly replicated DNA. *Genes Dev* 21(24):3342-55 doi:10.1101/gad.455407
- Neufert C, Becker C, Neurath MF (2007) An inducible mouse model of colon carcinogenesis for the analysis of sporadic and inflammation-driven tumor progression. *Nat Protoc* 2(8):1998-2004 doi:nprot.2007.279 [pii] 10.1038/nprot.2007.279
- Niture SK, Velu CS, Smith QR, Bhat GJ, Srivenugopal KS (2007) Increased expression of the MGMT repair protein mediated by cysteine prodrugs and chemopreventative natural products in human lymphocytes and tumor cell lines. *Carcinogenesis* 28(2):378-89 doi:bgl155 [pii] 10.1093/carcin/bgl155
- Nyskohus LS, Watson AJ, Margison GP, et al. (2013) Repair and removal of azoxymethane-induced O6-methylguanine in rat colon by O6-methylguanine DNA methyltransferase and apoptosis. *Mutat Res* 758(1-2):80-6 doi:10.1016/j.mrgentox.2013.10.001
- Ochs K, Kaina B (2000) Apoptosis induced by DNA damage O6-methylguanine is Bcl-2 and caspase-9/3 regulated and Fas/caspase-8 independent. *Cancer Res* 60(20):5815-24
- Quiros S, Roos WP, Kaina B (2010) Processing of O6-methylguanine into DNA double-strand breaks requires two rounds of replication whereas apoptosis is also induced in subsequent cell cycles. *Cell Cycle* 9(1):168-78
- R Development Core Team (2013) R: A language and environment for statistical computing. R Foundation for Statistical Computing, Vienna, Austria.
- Redon CE, Nakamura AJ, Zhang YW, et al. (2010) Histone gammaH2AX and poly(ADP-ribose) as clinical pharmacodynamic biomarkers. *Clin Cancer Res* 16(18):4532-42 doi:10.1158/1078-0432.CCR-10-0523
- Rosenberg DW, Mankowski DC (1994) Induction of cyp2e-1 protein in mouse colon. *Carcinogenesis* 15(1):73-8
- Roy L, Harrell CC, Ryan AS, Thorsteinsson T, Sancilio FD (2013) Development and Validation of a Single HPLC Method for Analysis of Purines in Fish Oil Supplements. *Food and Nutrition Sciences* 4(12):1255-1259 doi:10.4236/fns.2013.412160
- Ruvinsky A, Graves JAM (2005) *Mammalian genomics*. CABI Pub., Wallingford, UK ; Cambridge, MA
- Seiler F, Kirstein U, Eberle G, Hochleitner K, Rajewsky MF (1993) Quantification of specific DNA O-alkylation products in individual cells by monoclonal antibodies and digital imaging of intensified nuclear fluorescence. *Carcinogenesis* 14(9):1907-13
- Stephanou G, Vlastos D, Vlachodimitropoulos D, Demopoulos NA (1996) A comparative study on the effect of MNU on human lymphocyte cultures in vitro evaluated by O6-mdG formation, micronuclei and sister chromatid exchanges induction. *Cancer Lett* 109(1-2):109-14
- Stornetta A, Zimmermann M, Cimino GD, Henderson PT, Sturla SJ (2017) DNA Adducts from Anticancer Drugs as Candidate Predictive Markers for Precision Medicine. *Chem Res Toxicol* 30(1):388-409 doi:10.1021/acs.chemrestox.6b00380
- Thomas AD, Fahrner J, Johnson GE, Kaina B (2015) Theoretical considerations for thresholds in chemical carcinogenesis. *Mutat Res Rev Mutat Res* 765:56-67 doi:10.1016/j.mrrev.2015.05.001
- Thomas AD, Jenkins GJ, Kaina B, et al. (2013) Influence of DNA repair on nonlinear dose-responses for mutation. *Toxicol Sci* 132(1):87-95 doi:10.1093/toxsci/kfs341
- Tomaszowski KH, Schirrmacher R, Kaina B (2015) Multidrug Efflux Pumps Attenuate the Effect of MGMT Inhibitors. *Mol Pharm* 12(11):3924-34 doi:10.1021/acs.molpharmaceut.5b00341
- Trantakis IA, Nilforoushan A, Dahlmann HA, Stauble CK, Sturla SJ (2016) In-Geno Quantification of O(6)-Methylguanine with Elongated Nucleoside Analogues on Gold Nanoprobes. *J Am Chem Soc* 138(27):8497-504 doi:10.1021/jacs.6b03599
- Upadhyaya P, Lindgren BR, Hecht SS (2009) Comparative levels of O6-methylguanine, pyridyloxobutyl-, and pyridylhydroxybutyl-DNA adducts in lung and liver of rats treated chronically with the tobacco-specific carcinogen 4-(methylnitrosamino)-1-(3-pyridyl)-1-butanone. *Drug Metab Dispos* 37(6):1147-51 doi:10.1124/dmd.109.027078

- Vanden Bussche J, Moore SA, Pasmans F, Kuhnle GG, Vanhaecke L (2012) An approach based on ultra-high pressure liquid chromatography-tandem mass spectrometry to quantify O6-methyl and O6-carboxymethylguanine DNA adducts in intestinal cell lines. *J Chromatogr A* 1257:25-33 doi:10.1016/j.chroma.2012.07.040
- Wyss LA, Nilforoushan A, Williams DM, Marx A, Sturla SJ (2016) The use of an artificial nucleotide for polymerase-based recognition of carcinogenic O6-alkylguanine DNA adducts. *Nucleic Acids Res* 44(14):6564-73 doi:10.1093/nar/gkw589
- Xu-Welliver M, Pegg AE (2002) Degradation of the alkylated form of the DNA repair protein, O(6)-alkylguanine-DNA alkyltransferase. *Carcinogenesis* 23(5):823-30
- Zhang F, Bartels MJ, Pottenger LH, Gollapudi BB, Schisler MR (2006) Simultaneous quantitation of 7-methyl- and O6-methylguanine adducts in DNA by liquid chromatography-positive electrospray tandem mass spectrometry. *J Chromatogr B Analyt Technol Biomed Life Sci* 833(2):141-8 doi:10.1016/j.jchromb.2006.01.035
- Zhang J, Stevens MF, Bradshaw TD (2012) Temozolomide: mechanisms of action, repair and resistance. *Curr Mol Pharmacol* 5(1):102-14

FIGURE LEGENDS

Figure 1: Formation of O^6 -MeG DNA adducts and their analysis by qualitative and quantitative methods. **A** Formation of O^6 -MeG DNA adducts by alkylating agents. The anticancer drug temozolomide (TMZ) decomposes spontaneously to methyl-(triazen-1-yl) imidazole-4-carboxamide (MTIC) in aqueous solutions at pH > 7 (top panel). This unstable intermediate gives rise to 5-aminoimidazole-4-carboxamide (AIC) and diazomethane, which then reacts with nucleophilic centers in DNA, thereby forming O^6 -MeG DNA adducts. The colonotropic carcinogen azoxymethane (AOM), which is chemically related with N-nitroso compounds, requires metabolic activation by hepatic CYP2E1 to methylazoxymethanol (MAM). Subsequently, this compound undergoes decomposition to diazomethane as DNA methylating agent (bottom panel). MAM is also biliary excreted as glucuronic acid conjugate and thereby reaches the colorectum, where it also generates diazomethane (not shown). **B** Analysis of O^6 -MeG in cells and tissues. Please refer to the main text for further explanations.

Figure 2: Analysis of O^6 -MeG induction and persistence in CRC cells using immunofluorescence and mass spectrometry. **A** HCT116 cells were pre-treated with the MGMT inhibitor O^6 -Benzylguanine (O^6 -BG) for 2 h and then exposed to the anticancer drug TMZ (500 μ M) and incubated for up to 24 h. Representative images are shown. O^6 -MeG (green) and nuclei (blue). **B** Determination of the mean staining intensity by ImageJ. **C** Mass spectrometry-based detection of O^6 -MeG in HCT116 cells treated as described in A. Genomic DNA was isolated and O^6 -MeG levels were determined with mass spectrometry using an isotope-labeled internal standard. Data are depicted as mean \pm SEM (n=3). ****, p<0.0001; *, p<0.05; n.s. not significant. **D** Induction of O^6 -MeG adducts by 500 μ M TMZ with or without pre-treatment with the MGMT inhibitor O^6 -BG. Number of O^6 -MeG lesions were assessed by mass spectrometry. Data are shown as mean + SEM (n=3). Ns, not significant.

Figure 3: Detection of O^6 -MeG adducts in CRC cells by immunofluorescence. **A** HCT116 cells were pre-incubated for 2 h with O^6 -Benzylguanine to block cellular MGMT repair activity. Cells were then treated with increasing doses of the S_N1 -alkylating anticancer drug temozolomide (TMZ; 0 – 1000 μ M) for 2 h to allow for damage induction. Representative images acquired by confocal microscopy are shown. O^6 -MeG (green) and nuclei (blue). **B** Magnification showing pan-nuclear localization of O^6 -MeG adducts. **C** Quantitative evaluation of dose-response samples. Data are presented as mean + SEM (n=3, ≥ 10 sections per sample). ****, $p < 0.0001$.

Figure 4: Analysis of dose-dependent O^6 -MeG adduct formation in CRC cells by immune slot blot detection versus mass spectrometry. **A** HCT 116 cells were pre-incubated with the MGMT inhibitor O^6 -Benzylguanine (O^6 -BG) for 2 h and then challenged with increasing doses of the anticancer drug TMZ (0 - 1000 μ M) for additional 2 h. O^6 -MeG adducts were determined in isolated genomic DNA by an immune slot blot approach. Data are depicted as mean + SEM (n=3). ***, $p < 0.001$; *, $p < 0.05$; n.s. not significant. **B** Representative immuno-slot blot **C** Cells were treated as described in A and genomic DNA was isolated. The number of O^6 -MeG lesions per 10^7 nucleotides (nts) was obtained by mass spectrometry. Data are given as mean + SEM (n=3). ****, $p < 0.0001$; ***, $p < 0.001$; **, $p < 0.005$; *, $p < 0.05$.

Figure 5: Analysis of the dose-dependent O^6 -MeG formation in liver and colorectal tissue of MGMT-proficient and -deficient mice. Mass-spectrometry-based determination of hepatic (**A** and **C**) and colonic (**E** and **G**) O^6 -MeG lesions in isolated genomic DNA of WT and MGMT^{-/-} mice. Data with 10 mg AOM/kg bw has been reported previously by our group (Dörsam et al. 2018). Data is shown as mean + SEM (n = 3 per dose and genotype). ****, $p < 0.0001$; ***, $p < 0.001$; **, $p < 0.005$; *, $p < 0.05$.; n.s. not significant (as compared to the respective control treated with 0 mg AOM/kg bw). Dose-response modeling to elucidate the threshold dose for O^6 -MeG formation in liver (**B** and **D**) and colorectal (**F** and **H**) tissue of WT

and MGMT^{-/-} mice. Solid line shows the best fit of the model. The broken line shows the 90% lower confidence interval of the threshold dose for those dose-responses where linearity can be rejected.

TABLES

Table 1: SRM transitions for O^6 -MeG and O^6 -d3-MeG identification and quantification.

| | Quantification | | Qualification | |
|---------------|----------------|----------------------|----------------|----------------------|
| | SRM transition | Collision energy (V) | SRM transition | Collision energy (V) |
| Guanine | 152.1→135.1 | 26 | 152.1→110.1 | 26 |
| O^6 -MeG | 166.1→149.0 | 16 | 166.1→67.1 | 30 |
| O^6 -d3-MeG | 169.1→152.0 | 16 | 169.1→107.0 | 26 |

Table 2. Threshold dose analysis of *in vivo* samples. CI – confidence intervals

| Sample | Assay | Threshold dose (mg/kg bw) | Lower CI (mg/kg bw) |
|---------------------------|------------|---------------------------|---------------------|
| WT liver | ISB | - | - |
| MGMT ^{-/-} liver | ISB | - | - |
| WT Liver | UPLC-MS/MS | 1.93 | 0.78 |
| MGMT ^{-/-} liver | UPLC-MS/MS | - | - |
| WT colon | UPLC-MS/MS | 4.78 | 3.20 |
| MGMT ^{-/-} colon | UPLC-MS/MS | 1.32 | 0.00 |

Table 3: Features of the different analytical techniques used for O^6 -MeG detection.

| | Immunofluorescence | Immuno-slot blot | UPLC-mass spectrometry |
|-----------------|--------------------|------------------|------------------------|
| Required sample | ≤ 50.000 cells | 250 - 500 ng DNA | ≥ 5 µg DNA |
| Sensitivity | Moderate | Moderate | High |
| Specificity | Moderate | Moderate | High |
| Throughput | Moderate | High | Low |

FIGURES

Figure 1

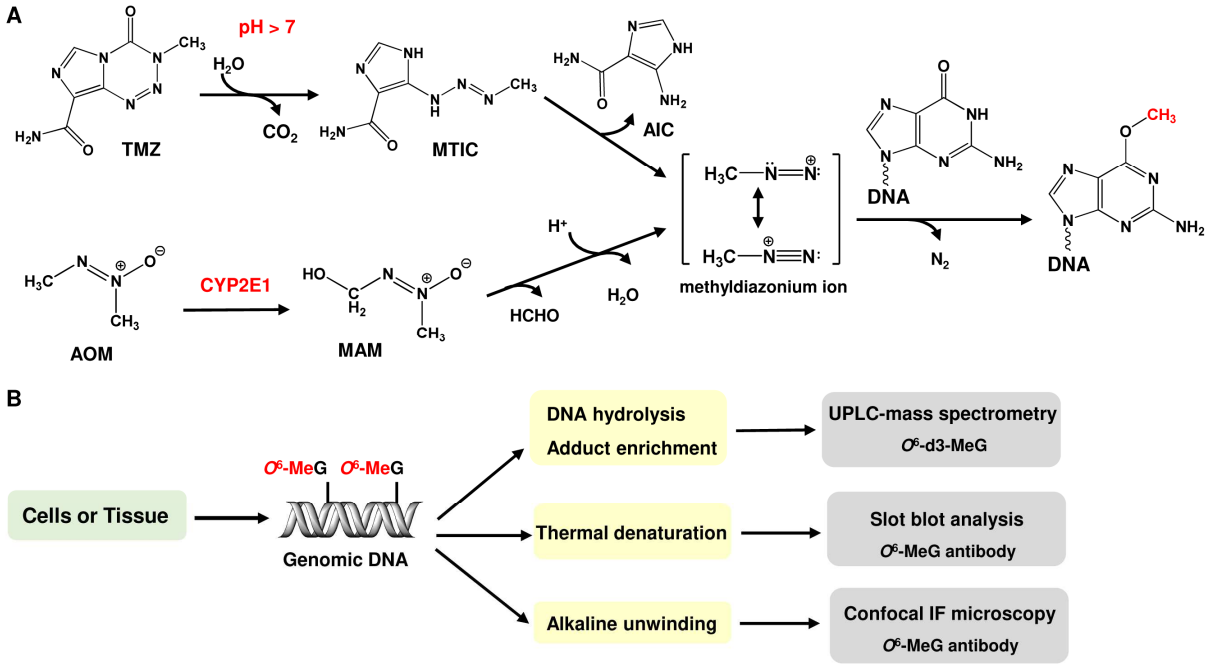


Figure 2

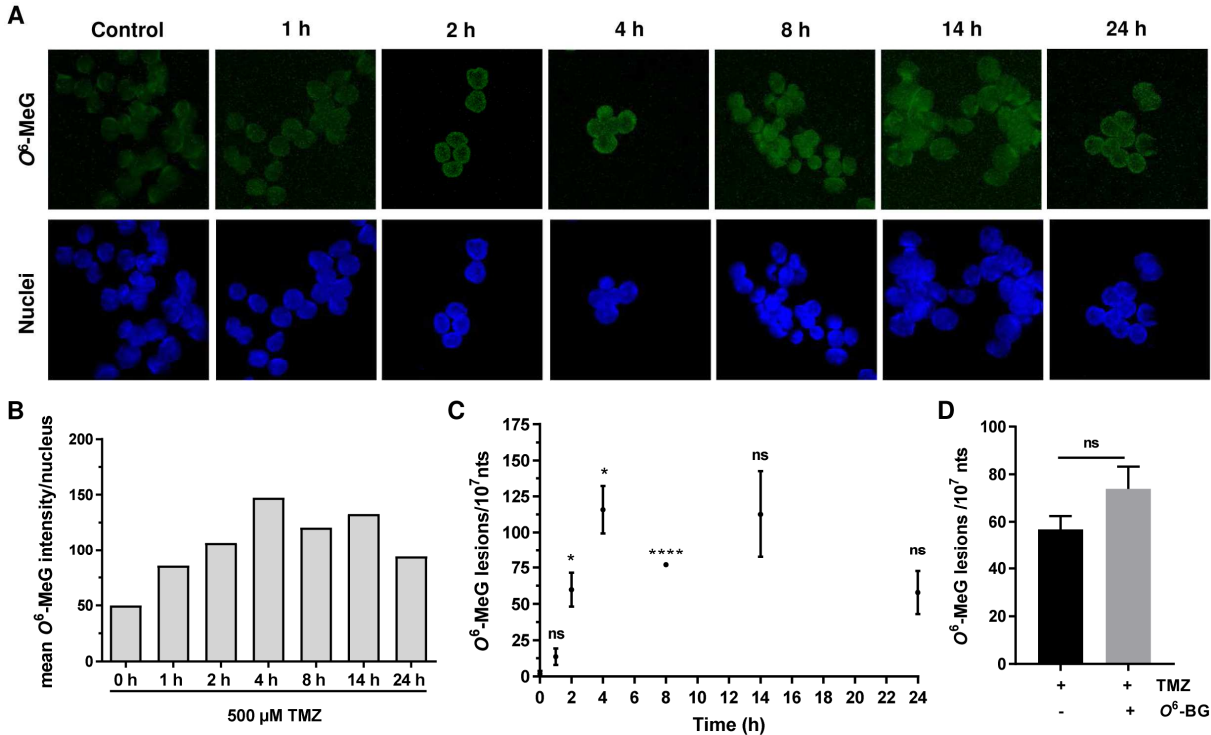


Figure 3

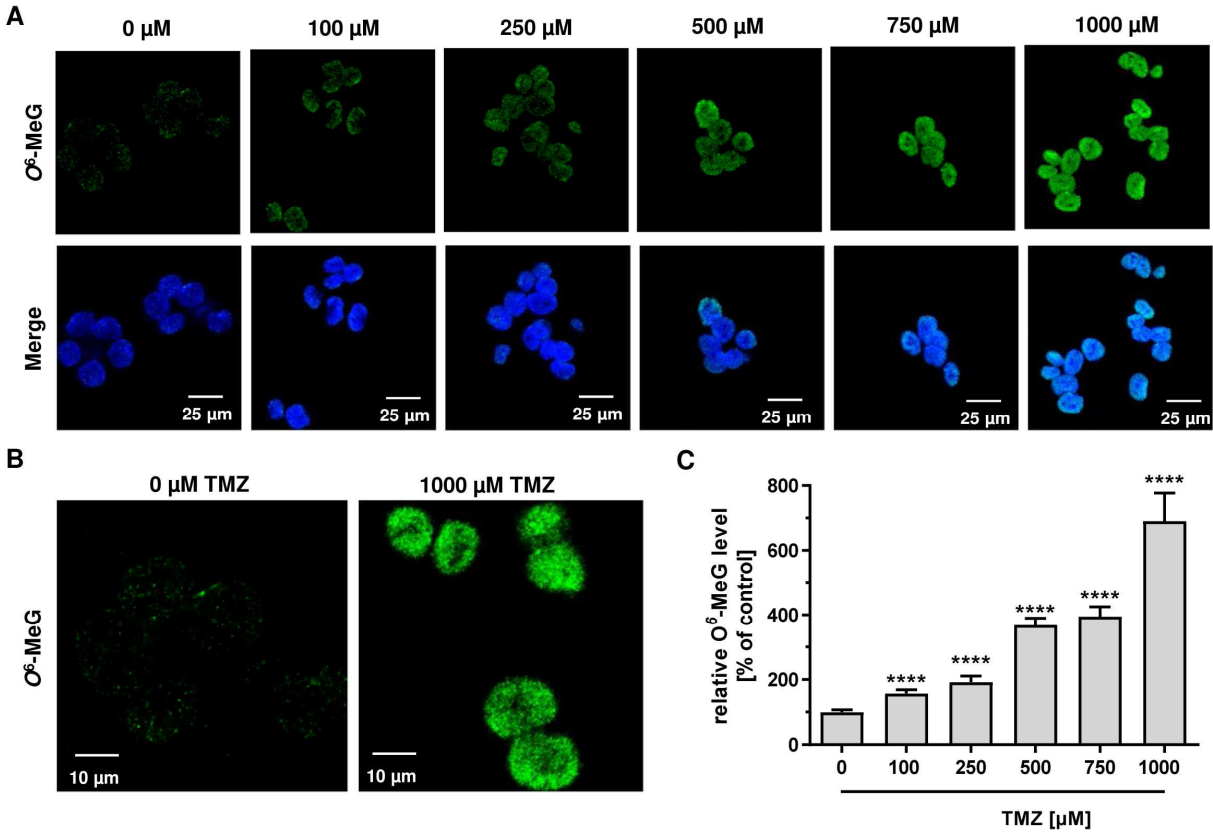


Figure 4

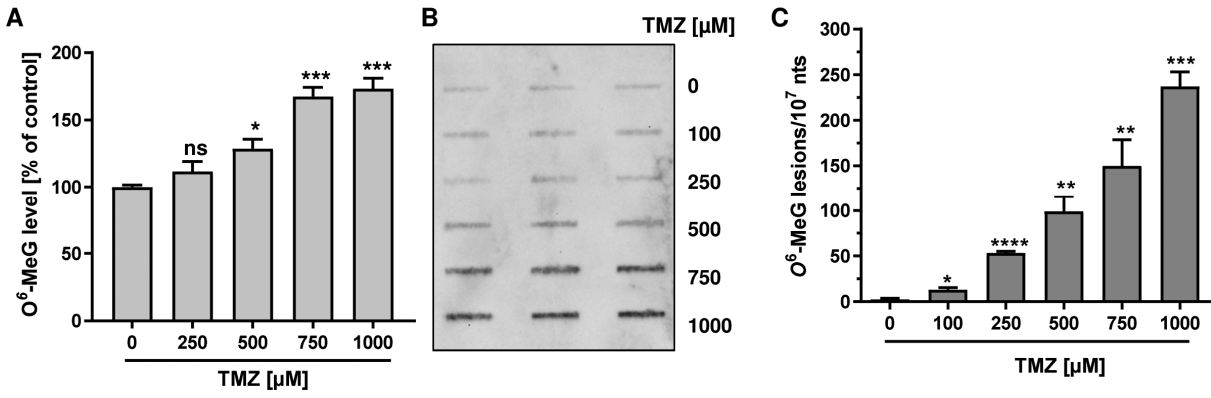


Figure 5

